AIP Advances

Impact of pearl-necklace-like skeleton on pore sizes and mechanical properties of porous materials: A theoretical view

Cite as: AIP Advances **12**, 105108 (2022); https://doi.org/10.1063/5.0112914
Submitted: 28 July 2022 • Accepted: 12 September 2022 • Published Online: 11 October 2022

Ameya Rege, Shivangi Aney and Lorenz Ratke

COLLECTIONS

This paper was selected as an Editor's Pick

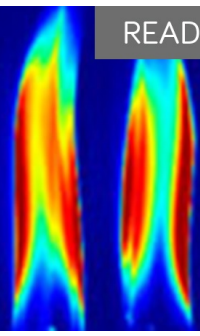

AIP Publishing

Impact of pearl-necklace-like skeleton on pore sizes and mechanical properties of porous materials: A theoretical view

Cite as: AIP Advances 12, 105108 (2022); doi: 10.1063/5.0112914
Submitted: 28 July 2022 • Accepted: 12 September 2022 •
Published Online: 11 October 2022

Ameya Rege,[1,2,a] Shivangi Aney,[1] and Lorenz Ratke[1]

AFFILIATIONS

[1] Department of Aerogels and Aerogel Composites, Institute of Materials Research, German Aerospace Center, Linder Höhe 51147, Cologne, Germany
[2] School of Computer Science and Mathematics, Keele University, Staffordshire ST5 5BG, United Kingdom

[a] Author to whom correspondence should be addressed: ameya.rege@dlr.de

ABSTRACT

The structural and mechanical properties of open-porous cellular materials are often described in terms of simple beam-based models. A common assumption in these models is that the pore walls have a constant cross section, which may be in agreement for a vast majority of such materials. However, for many of those materials that are characterized by a pearl-necklace-like network, this assumption seems too idealized. Aerogels are perfect examples of such materials. In this paper, we investigate the effect of such pore walls having a string of pearls-like morphology on the properties of such open-porous materials. First, the pore size is mathematically modeled. Three scenarios are described, where the pore sizes are calculated for cells in 2D, 3D, and 3D with overlapping particles. The dependency of the skeletal features on the resulting pore size is investigated. In the second part, pore walls with 3D overlapping spheres are modeled and subjected to axial stretching, bending, and buckling. The effect of the particle sizes and the amount of overlap between the particles on the mechanical features is simulated and illustrated. The results are also compared with models that assume a constant cross section of pore-walls. It can be observed that neglecting the corrugations arising from the pearl-necklace-like morphology in open-porous cellular materials can result in serious miscalculations of their mechanical behavior. The goal of this paper is not to quantify the bulk mechanical properties of the materials by accounting for the pearl-necklace-like morphology but rather to demonstrate the significant deviations that may arise when not accounted for.

I. INTRODUCTION

The cellular models proposed by Gibson and Ashby[1,2] for 3D (as well as 2D) open-porous cellular materials can describe the properties of a large body of data on honeycomb-like structures and diverse foams. Inspired by natural cellular materials, such as wood, cork, and bone, many man-made cellular porous materials, e.g., polymeric foams and aerogels, have emerged in the last decades. To exploit the optimum combination of properties of such materials, one has to carefully describe the relationship between the pore-structure and, subsequently, the mechanical and thermal characteristics as functions of their density and pore features, so that designing specific properties can be realized. The models proposed by Gibson and Ashby work fine and have contributed toward the understanding of the relationship between the properties of foam material and their densities. These were possible because most materials on which the theory was applied did show a cellular pore-structure with a constant cross section of pore walls. Therefore, the pore-walls may be assumed to be quadratic or cylindrical. Another interesting feature in many porous materials is their pore-size distribution. For a vast majority of foams as well as for honeycomb-like structures, this remains nearly constant. On the other hand for materials like aerogels, the pore sizes can range from a few nanometers to hundreds of nanometers or even micrometers. Accounting for the pore-sizes and perhaps even harmonizing them remains an important factor in tailoring the thermal[3] and mechanical[4,5] properties of such materials. Specifically focusing on the mechanical properties, Rege *et al.*[4] have modeled these by

proposing a micromechanical constitutive model for cellular materials having a wide pore-size distribution. The model accounts for the variation in the pore sizes, by introducing the distribution function in the constitutive model. The application of the model to different aerogels was also shown.[6,7] However, in these models, the pore walls were assumed to have a constant cross section. This was justified for the modeled aerogels because they featured a fibrillar morphology having a more or less constant cross section. However, in the cases of silica or organic aerogels, this remains far from the truth. Therefore, the pore walls have the appearance as that of a string of pearls. However, some models have attempted to describe the mechanical properties of such materials by using 2D or 3D models where the pore walls had constant cross sections.[8–10] In particular, models such as the one proposed by Lei and Liu[9] in an attempt to characterize silica aerogels, where they account for the dead-ends while still assuming a cube-shaped unit cell with a constant cross section of the pore walls, still obtained a scaling exponent of 2.04 in the relation $E \propto \rho^m$. In materials like aerogels, it is not the dead-ends or a lack of their presence that dictate the unusual mechanical properties, but it is rather the random connectivity and the effect of the pearl-necklace-like morphology. While a few authors have investigated the effect of the random connectivity on the mechanical properties,[11,12] the effect of the pearl-necklace-like morphology remains nearly unattended.

There is not a significant amount of literature on the modeling of the mechanics of porous materials by considering the inter-particle necks. The terminology of pearl-necklace-like structures arises from polymers[13] and proteins.[14] However, the use of this terminology for porous materials like aerogels is now well established.[15–17] The effect of inter-particle necks on the morphological and elastic properties of porous ceramic films was studied by Chen *et al.*[18] They investigated the influence of inter-particle neck sizes on the mechanical properties and the effects arising from coarsening of the network structure. Therefore, post-processed tomographic images were used in a finite element program for such analysis. Colloidal materials generally show such arrays of particles forming interconnected networks. The mechanical behavior of such arrays of particles describing the backbone of a colloid has been described by Dargazany and Itskov.[19] They further showed the possibility to model the arrays of particles as nonlinear springs.[20] Over the validity of modeling inter-particle necks as linear springs, Dargazany *et al.*[21] reported that for moderately connected bonds, the assumption may remain valid. In the case of many aerogels, the arrays of particles consist of moderately connected bonds, which was the motivation by Aney *et al.*[10] to model the arrays of particles in resorcinol-formaldehyde (RF) aerogels as beams. This was also done earlier by Schwan *et al.*[8] to model the flexibility in RF aerogels. As seen from both these studies, in the case of most aerogels, the pore collapse occurs as a result of critical stress arising from buckling or bending of the pore walls, which leads to subsequent failure of the arrays of particles, which may then end in crack formation. Since the kinematics of both these deformation modes is dependent on the area moment of inertia of the pore walls, the effect of particle necks must be significant.

This paper attempts to describe and analyze the importance of considering the pearl-necklace-like pore-wall as against the one with a constant cross section, for correct interpretation of the pore sizes and the mechanical properties. To this end, mathematical descriptions of the pore space based on simple 2D and 3D models are presented. Additionally, for the 3D case, the effect of overlapping spheres is also considered. The latter case is also then applied in a finite element framework to simulate the mechanical behavior of the pore walls. To this end, the three basic modes of deformation are studied, such as axial stretching, bending, and buckling. All results are compared with the case of a constant cross section of the pore wall.

This paper is organized as follows: In Sec. II, the methods used for modeling are described. First, the mathematical modeling of the pore spaces is elucidated, and then, the computational model for studying the mechanical properties is detailed. In Sec. III, the results from both, the model for pore sizes and its implementation in the finite element program, are illustrated and discussed. Finally, a conclusion is presented in Sec. IV.

II. METHODS

A. Mathematical description of the pore sizes

In this section, we present mathematical formulations of the pore sizes on the basis of simple cubic-shaped lattices, having particles of diameter d. To estimate the pore sizes, the free space in the enclosed volume is calculated. In order to model aerogel-like materials, the eight particles at the vertices of a simple cubic lattice are pushed further away by adding particles on each edge. This means the distance between the particles at the vertices is extended. This automatically leads to a reduction of solid fraction and an increase in pore sizes. We first begin with a simple 2D model and then move toward the 3D ones.

1. 2D model

The square shaped 2D cell is sketched in Fig. 1. For a simple cubic lattice, the area fraction of circles within the dashed square shown in Fig. 1 is

$$F_s = \frac{\pi}{4} d^2. \tag{1}$$

The cell area of the square is

$$F_c = d^2, \tag{2}$$

and thus, the solid fraction can be calculated as

$$\phi_s^{2D} = \frac{\pi}{4}. \tag{3}$$

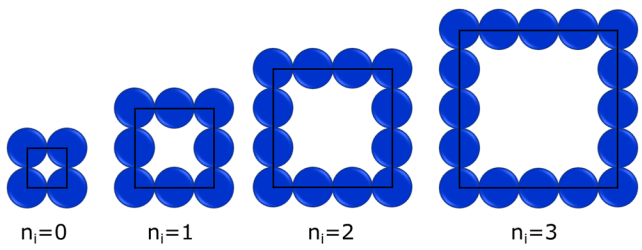

FIG. 1. Illustration of 2D cells with increasing n_i.

Whenever we add a particle on the edge, the cell size increases, and the area fraction of particles within the cell increases too. This can be calculated for n_i inserted particles as

$$F_s = (2n_i + 1)\frac{\pi}{4}d^2, \tag{4}$$

and the area of the cell changes to

$$F_c = (n_i + 1)^2 d^2, \tag{5}$$

and thus, subsequently, the solid fraction can be calculated as

$$\phi_s^{2D} = \frac{F_s}{F_c} = \frac{\pi}{4}\frac{2n_i + 1}{(n_i + 1)^2}. \tag{6}$$

In open-porous materials like aerogels, the solid fraction (equivalent to the envelope density divided by the skeletal density) is fixed and typically below 10%. We can solve Eq. (6) for n_i, since it is a simple quadratic equation. In reality, for a very small solid fraction, the number of inserted particles in a cell must be large. For $n_i \gg 1$, we can simplify Eq. (6) to

$$\phi_s^{2D} \cong \frac{\pi}{2n_i} \text{ or } n_i \cong \frac{\pi}{2\phi_s^{2D}}. \tag{7}$$

The pore size can then be roughly estimated as the size of a square bounded by the particles on the edges, which yields

$$d_p \approx \frac{\pi}{2\phi_s^{2D}}d. \tag{8}$$

Therefore, for a decreasing solid fraction, the pore size becomes larger in a hyperbolic manner as long as the particle size remains fixed. For materials whose pore size is nearly the same as that of the size of the particles, one could directly use Eq. (6); for example, for $n_i = 1$, one obtains $d_p \approx 2.66d$. One could now also calculate the specific surface area and other properties. However, it is interesting to analyze the same for the 3D problem, which is more realistic.

2. 3D model

Although in 3D, the idea remains the same, and the resulting equations look quite different. The idea is sketched in Fig. 2. The volume of a sphere at each vertex contributes 1/8th to the volume inside the cell box going through the centers of the spheres. The volume at each vertex is

$$V_{\text{vertex}} = \frac{1}{8}\frac{\pi}{6}d^3. \tag{9}$$

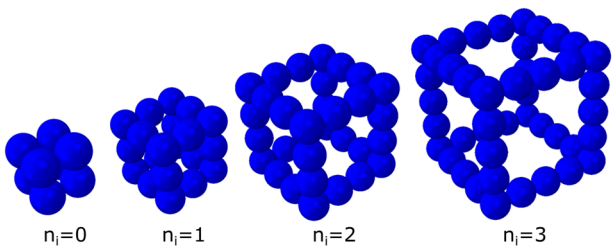

FIG. 2. Illustration of 3D cells with increasing n_i.

Therefore, the contribution to the total solid volume in the box is

$$V_{\text{vertices}} = 8\left(\frac{1}{8}\frac{\pi}{6}d^3\right). \tag{10}$$

The box volume $V_b = d^3$; thus, the solid fraction of a simple cubic lattice is

$$\phi_s^{3D} = \frac{\pi}{6}. \tag{11}$$

Comparing this to the 2D case as treated above, it is smaller. Each inserted sphere at the edges adds to the solid fraction of a volume,

$$V_{ii} = \frac{1}{4}\frac{\pi}{6}d^3, \tag{12}$$

and since there are 12 spheres to be added, we have

$$V_i = \frac{\pi}{2}d^3. \tag{13}$$

The box volume increases, since the edge length increases to a value of $2d$, and thus, the solid fraction decreases. If we insert n_i, $i = 0, 1, 2, 3, \ldots$, spheres on the edges, the volume added is

$$V_i = n_i\frac{\pi}{2}d^3, \tag{14}$$

and the edge length increases to $d_b = (n_i + 1)d$, and thus, the volume increases to

$$V_b = (n_i + 1)^3 d^3. \tag{15}$$

The total volume inside the box is then that of the spheres on the edges plus that at the vertices,

$$V_s = \frac{\pi}{6}d^3(1 + 3n_i). \tag{16}$$

The solid fraction is then

$$\phi_s = \frac{\pi}{6}\frac{(1 + 3n_i)}{(n_i + 1)^3}. \tag{17}$$

Again, for materials with d_p and d of the same order, one could use this equation directly. At large n_i, we can simplify this expression to

$$\phi_s^{3D} \approx \frac{\pi}{2}\frac{1}{n_i^2}. \tag{18}$$

Now one can compare this result with the one from Eq. (7) and observe that the dependence is much different from the 2D case, where it was hyperbolical. If we again simply calculate the pore size in these open cubes as that of an inserted cube, we get for $n_i \gg 1$,

$$d_p = n_i d \approx \sqrt{\frac{\pi}{2\phi_s^{3D}}}d. \tag{19}$$

In contrast to the 2D case, the pore size increases only like the inverse square root with the volume of the solid fraction (equivalent to the envelope density). This also sheds some light on the quantitative deviations that may result in modeling 3D porous networks, assuming merely 2D models.

3. Overlapping 3D model

In more real aerogel-like materials, the particles do not touch only at a point, but a neck develops at the point of contact, giving an impression that the spheres overlap to a certain amount. One can imagine the following situation: Particles form in the gel solution, either by nucleation or by phase separation, and move in the solvent and touch (diffuse). Once they touch, they will immediately establish bonds, either covalent ones, hydrogen, or ionic. In any case, they then move as dumbbells or later as clusters of many particles. Since the solvent is still rich in monomers, oligomers, etc., these will attach to the particles and the dumbbells, and they would grow. At their area of contact or better at the circular contact line, they preferably condense since the effect of concave curvature increases the condensation or attachment rate (since the bonding energy gain becomes larger). Therefore, the particles or their clusters grow in an onion-like manner, and the necks grow in size too. After gelation and drying, the aerogel made from them looks as if the particles just would only overlap, and spheres would have penetrated into each other. The formation of necks of contacting particles in a network is a quite general phenomenon of particulate porous bodies and treated for instance in the literature on sintering of metals and ceramics.[22,23] Neck formation and growth of a particulate aggregate in a liquid environment are always due to the dependence of solute solubility on the radius of curvature. A solute is dissolved at convex parts of a surface and precipitates at concave parts. This leads to a growth of the neck radius for particles being in contact. In wet gels, the situation is a bit different, as described above, since the pore liquid of a gel network still contains monomers and oligomers after gelation, which preferably condense at concave surface areas and thus stiffen the network. In the sol–gel literature, this phenomenon always is termed aging, and there exists a huge amount of literature on the effect of aging on the microstructure of gels and aerogels.[24–31] Detailed mathematical models of neck formation and growth are not developed for gels, which can be transformed into aerogels. We, therefore, discuss the necks between contacting particles, which are simply geometrical as overlapping spheres.

Figure 3 shows the same arrangement as in Fig. 2, but here, the overlap is allowed. In principle, spheres that overlap can be treated as if spherical caps are removed from them. The cap shall have a height h as shown in Fig. 4. The cap volume of a sphere with radius R can be calculated as

$$V_{\text{cap}} = \frac{\pi}{3}h^2(3R-h) = \frac{\pi}{3}\xi^2R^3(3-\xi), \tag{20}$$

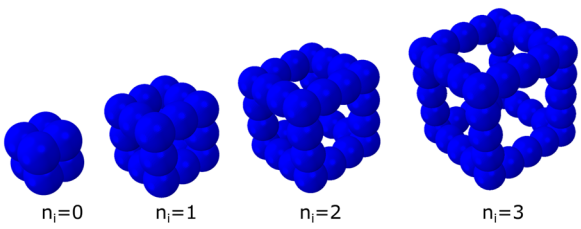

FIG. 3. Illustration of 3D cells with overlaps with increasing n_i.

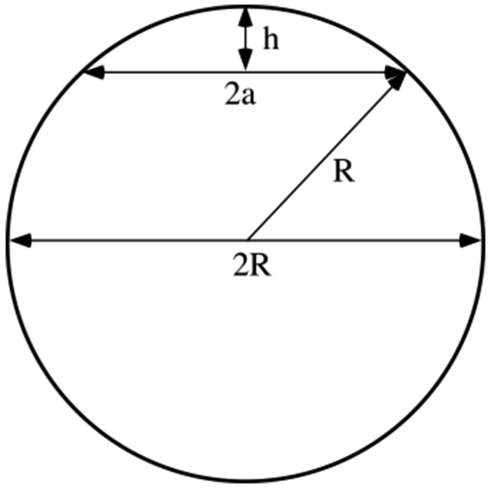

FIG. 4. Illustration of the overlap of height h for a particle with radius R.

with the then obvious definition of the overlap as $\xi = h/R$. We calculate again the volume of spheres at the vertices and then that of spheres inserted at the edges. The volume of a sphere contributing to the solid fraction inside the cube defined by the centers of the spheres at the vertices is

$$V_{\text{vertex}} = V_{\text{sphere}} - 6V_{\text{cap}} = \frac{4\pi}{3}R^3\left(1-\frac{3}{2}\xi^2(3-\xi)\right). \tag{21}$$

The volume of a sphere inserted along the edge equals that of a sphere minus two times a cap, and thus,

$$V_i = \frac{4\pi}{3}R^3\left(1-\frac{1}{2}\xi^2(3-\xi)\right). \tag{22}$$

Each sphere at the vertex adds only 1/8th of its volume to the solid fraction inside a cube. We have eight vertices, and thus, the total volume is already given by the expression of Eq. (21). Along the 12 edges, we can add n_i spheres, each adding 1/4th of its volume to the solid fraction, and thus, we obtain for the total volume inside the cube as

$$V_{\text{total}} = \frac{4\pi}{3}R^3\left(1-\frac{3}{2}\xi^2(3-\xi)\right) + 3n_i\frac{4\pi}{3}R^3\left(1-\frac{1}{2}\xi^2(3-\xi)\right). \tag{23}$$

The cube or quadratic box has a side length (with $d = 2R$) of

$$d_c = (n_i+1)d(1-\xi), \tag{24}$$

and thus, a volume of

$$V_c = 8R^3(n_i+1)^3(1-\xi)^3. \tag{25}$$

The solid fraction is then

$$\phi_s = \frac{\pi}{6}\frac{\left(1-\frac{3}{2}\xi^2(3-\xi)\right)+3n_i\left(1-\frac{1}{2}\xi^2(3-\xi)\right)}{(n_i+1)^3(1-\xi)^3}, \tag{26}$$

where as before, if we only consider $n_i \gg 1$, the relationship simplifies to

$$\phi_s \approx \frac{\pi}{2n_i^2}\left(\frac{1-\frac{1}{2}\xi^2(3-\xi)}{(1-\xi)^3}\right). \tag{27}$$

Assuming that the overlap is small, we can develop the fraction around $\xi = 0$ to the second order and yield

$$\phi_s = \frac{\pi}{2n_i^2}\left(1+3\xi+\frac{9}{2}\xi^2\right). \tag{28}$$

Thus, the pore size can be expressed as

$$d_p = n_i d(1-2\xi) = d(1-2\xi)\sqrt{\frac{\pi}{2\phi_s}\left(1+3\xi+\frac{9}{2}\xi^2\right)}. \tag{29}$$

B. Computational model of the mechanical properties

To investigate the effect of such pearl-necklace-like networks on the mechanical properties, we directly use the proposed case of overlapping spheres. Generally, microstructure-based models on aerogels studying their mechanical properties assume the cellular network to be made up of idealized square-shaped 2D cells or cube-shaped 3D ones.[4,9] Rege *et al.*[4] recently proposed a generalized micromechanical model for describing the mechanical properties of cellular materials, either in an elastic or an inelastic setting. The mode was based on the failure modes proposed by Gibson and Ashby.[2] The proposed model accounts for the variation in the cell sizes but assumes a constant cross section of the pore-walls while accounting for the axial and bending effects under mechanical loads. Since the pore sizes show a strong influence on the presence of spherical particles, it is interesting to understand the influence of the pearl-necklace-like structure on the mechanical properties. It should be noted that the goal of this paper is not to quantify the bulk behavior or properties of open-porous materials exhibiting a pearl-necklace-like morphology but to merely show the local effects and quantify their significance while describing the pore-wall kinematics. To this end, the pore walls are modeled for different ξ values.

Figure 5 illustrates the considered models. Different values of ξ are considered, ranging from 1/8 to 3/4, and are compared

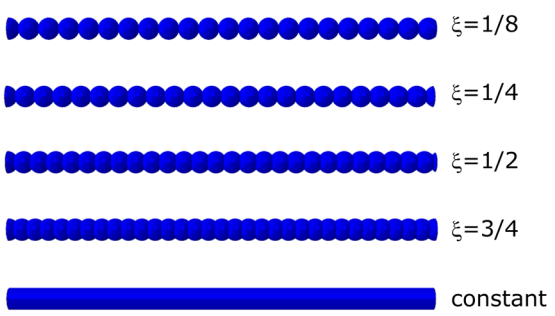

FIG. 5. Simple pore-wall geometries considering the overlapping of particles in a pearl-necklace-like network.

to the results of the constant cross section. Typically, for aerogel-like materials, a ξ value up to 1/4 seems realistic. A ξ of 1/2 or 3/4 is usually not observed in scanning electron micrographs of aerogels. However, for the sake of completeness of the study, these are considered. The presented models are subjected to axial stretching, bending, and buckling in a finite element setting. The mechanical properties are investigated not only for different ξ values but also for three different particle sizes d. Thus, not only the effect of overlaps but also correspondingly that of the particle sizes is studied. All simulations were carried out on ABAQUS. A simple linear elastic model, with a Young's modulus of 1.5 GPa and a Poisson ratio of 0.3, was used for all simulations. Solid element type C3D8R, which is a general purpose brick element with reduced integration, was used. The element type with reduced integration was used to avoid the locking phenomena. The axial stretching and bending simulations were conducted by means of a general static step, while buckling was analyzed by means of the linear perturbation procedure.

III. RESULTS AND DISCUSSION

The results from the calculations of the pore sizes are first discussed. Figure 6(a) illustrates the results from the 2D calculations. It can be seen that the relationship between the pore size and the solid fraction is of a hyperbolic nature for a constant particle diameter. Thus, the smaller the solid fraction, the larger the pore size. For solid fractions <0.2, the pore sizes strongly increase with a minor decrease in the solid fraction. This change becomes less significant for larger solid fractions. For aerogel-like materials, the solid fractions are almost always <0.2, even <0.1 in most cases. With increasing particle diameters, the pore sizes increase, while retaining the nature of the curve. Three particle diameters, 4, 8, and 16 units, were considered. In the case of 3D, however, while the trend can be seen to be the same, the nature is very different [see Fig. 6(b)]. Due to the presence of the square-root in the relationship between the pore size and the solid fraction [eq. (2.19)], the decrease in pore size is much less stronger with increasing solid fraction. For the same size of the pore walls, one can also observe that the pore sizes are reduced by a factor of over five. This emphasizes the need to describe 3D pore-structured materials using 3D models and not simplify using 2D assumptions. To investigate the effect of the overlap, a constant diameter of 8 units was considered, and the overlap factor ξ was varied from 1/16 to 1/4 [see Fig. 6(c)]. Compared with the no overlap results for a diameter of 8 units from Fig. 6(b), it can be inferred that with increasing overlap, the pore size decreases. However, the nature of the relationship remains the same. Since the length of the pore walls in a considered 2D or 3D pore remains an important morphological feature for modeling a unit cell, its influence on the solid fraction remains crucial for pore size estimation. Figure 6(d) shows the effect of increasing the number of particles in the pore wall on the solid fraction. While the trend in the 2D and 3D cases seems similar, the decrease in the solid fraction with an increasing number of particles for the 3D case is much stronger than that in 2D. For larger n_i, the role of overlaps is minimal in dictating the solid fraction. The results illustrated in Fig. 6 demonstrate that the morphology of the pore walls plays an important role in driving the pore space. Furthermore, the influence of the solid fraction on the pore sizes can be effectively modeled by assuming simple geometric pore shapes. The

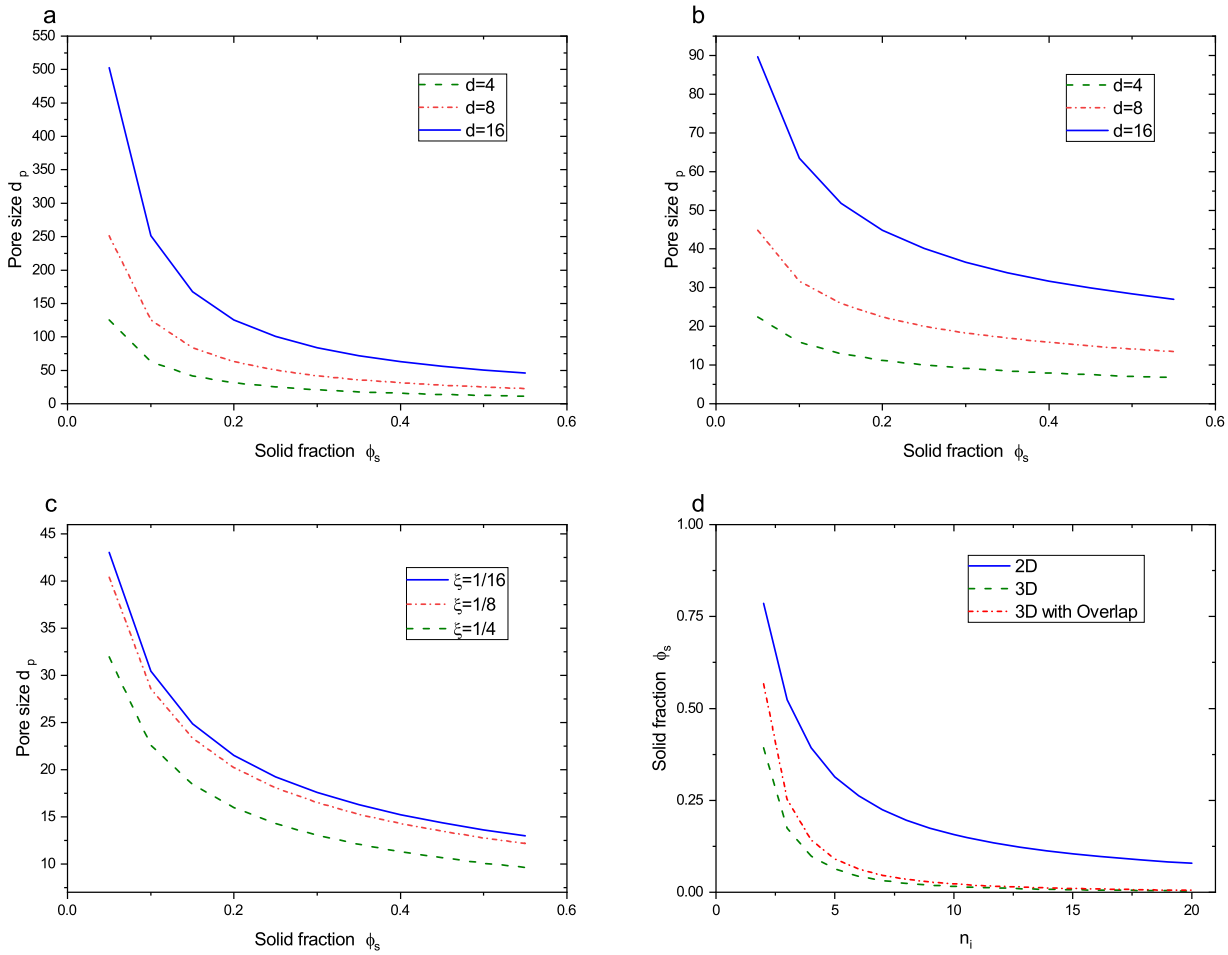

FIG. 6. Effect of a solid fraction on the pore sizes for (a) 2D, (b) 3D, and (c) 3D with overlap models. Here, in sub-figures (a) and (b), particle sizes of 4, 8, and 16 units are modeled. In sub-figure (c), a particle size of 8 units is modeled with three overlap factors of 1/16, 1/8, and 1/4. (d) The effect of the number of particles in a pore wall on the solid fraction for all three cases. Note the change in the magnitude of the y axes in sub-figures (a) and (b) as well as (c).

influence of overlaps, which is typical in aerogel-like materials, can also be captured.

While the presence of a string of pearls and the inter-particle necks show significant influence on the porous space of the materials, their effect on the mechanical properties of the pore walls must be non-negligible. This is because the mechanical properties of cellular materials are dictated by their skeletal features.[32] Figure 7 illustrates the effect of considering (overlapping) particles against the constant cross section on the different modes of deformation in a typical pore wall of an open-porous cellular material, namely, axial stretching, bending, and buckling. Four cases of overlaps, ranging from $\xi = 1/8$ to $\xi = 3/4$, are considered. Figure 7(a) shows the deformed pore walls for all ξ cases as well as the case with the pore wall having a constant cross section subjected to axial stretching. To model axial stretching, the pore-wall was fixed on one end, and a force was applied on the other. Stress concentrations can be observed at the inter-particle necks, while most of the particle volume remains stress free in the rest of the places. Figure 7(b) shows that assuming a constant cross section of the pore wall can result in severe underestimation of the maximal axial stress. This might result in underestimating the failure in the materials network. It can also be inferred that the smaller the overlap, the larger the axial stresses. This can be attributed to the smaller particle necks giving rise to high stress concentrations. Thus, the smaller the particle necks, the sooner would the pore wall fails under stretching. The significance of modeling the particles and their necks is thus demonstrated. This is reflected even in the case of bending. Figure 7(c) shows the deformed pore walls under bending, while Fig. 7(d) shows the maximal bending stress vs the overlap. To model the bending in the wall, a cantilever model was chosen, where one end of the pore wall was fixed, and the other was subjected to a single force. Also in this case, one observes that assuming a constant cross section severely underpredicts the bending stress in the pore walls. The factor is much larger than in the case of axial stresses.

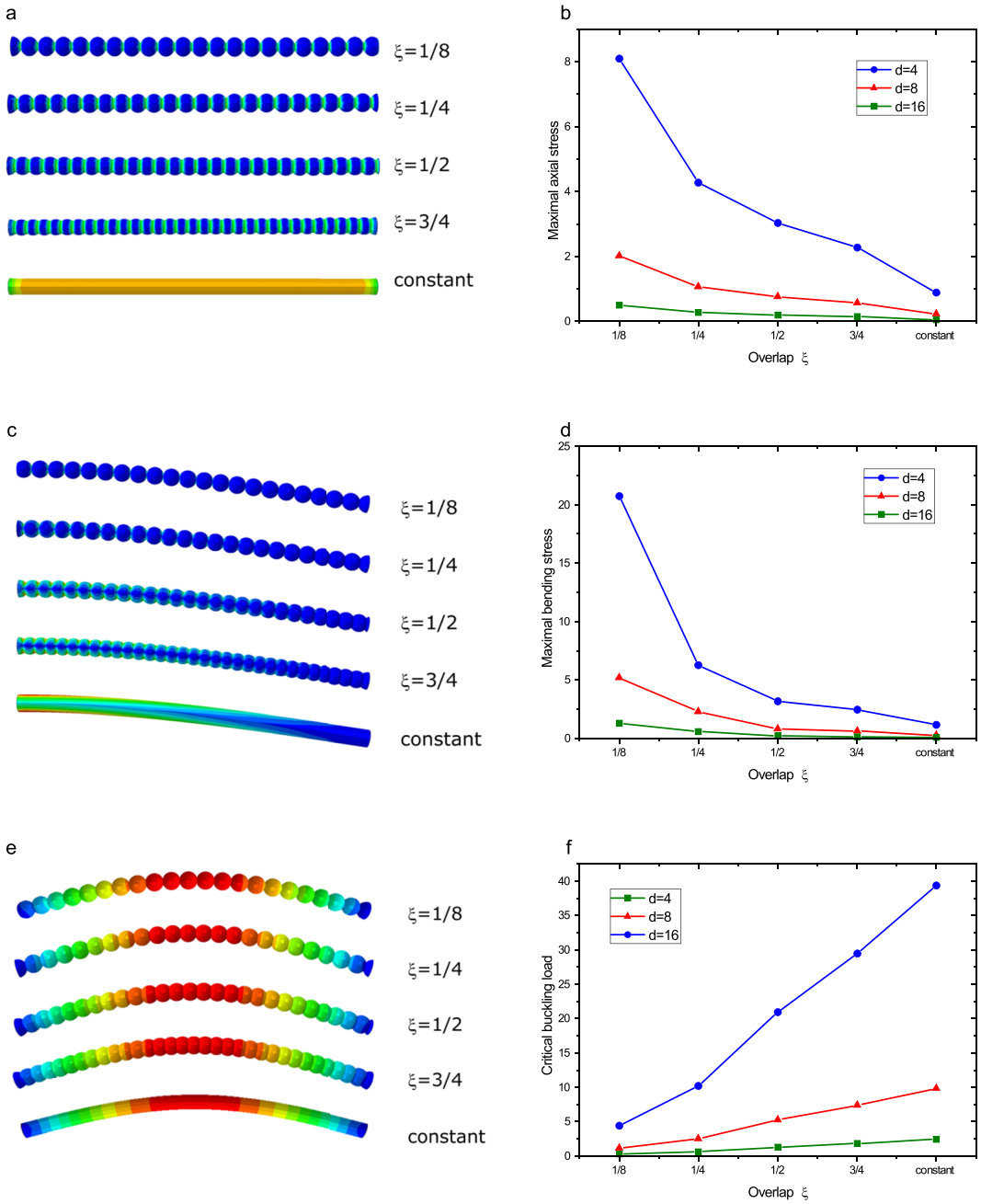

FIG. 7. Illustration of the different deformation scenarios in the pore-walls, with constant as well as overlapping pearl-necklace-like cross sections. Pore-wall under (a) axial stretching, (c) bending, (e) buckling, and (b), (d), and (f) their corresponding stress/force vs overlap for different particle radii. Each investigated deformation scenario is modeled for three *d* values, namely, 4, 8, and 16 units, and with varying overlap factors.

Moreover, as expected from the classical theory, the thinner the beam, the larger the deflection and the lower the stresses. This can be inferred from the simulations with different particle diameters, while also from the different constant cross-sectional models with different diameters. In the last case, the effect of particle necks on buckling behavior is demonstrated. Figure 7(e) shows the pore walls subjected to buckling. Euler's buckling criteria with the column effective length factor equal to 1 was modeled. It can be inferred from Fig. 7(f) that the smaller the overlap, the smaller the critical buckling load. Thus, assuming a constant cross section would result in a delayed

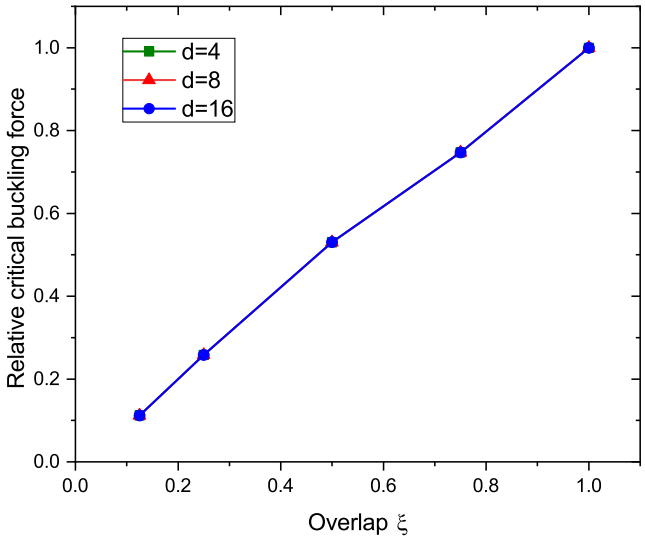

FIG. 8. Relative critical buckling force vs overlap for different particle radii.

prediction of pore collapse. The results inferred from Fig. 7(f) were further handled to check the effect of the particle sizes and the overlap on the relative critical buckling load. This relative load is calculated by dividing the critical buckling force in Fig. 7(f) by the critical load in the case of a constant cross section. The results are plotted in Fig. 8. It can be realized that all the curves for different particle sizes coalesce, thus inferring that the critical buckling load simply scales linearly with ξ.

The results in Fig. 7 demonstrate the importance of considering the pearl-necklace-like structure in theoretically describing the mechanical properties of open-porous materials having a similar morphology. While only local effects at the pore-wall level can be deduced from this analysis, it opens up an important question on the validity of assuming a constant cross section for the pore walls while modeling such networks. Considering constant cross sections in the case of stretching and bending results in modeling a sooner failure in the walls, while in the case of buckling, the pore collapse may be modeled too late. Furthermore, the factor of differences in the stresses/loads are significantly large, thus making their accountability unavoidable. While these presented results are very promising in describing the necessity of accounting for such pearl-necklace-like models, e.g., the overlapping sphere model described in this work, it is also interesting to see the effect on the bulk elastic properties as functions of the local skeletal features. This will be investigated in a subsequent study.

IV. CONCLUDING REMARKS

In this paper, the effect of pearl-necklace-like models on the pore sizes and the mechanical properties of porous materials is investigated. By means of mathematical relations, it was shown that the pore sizes decrease in a hyperbolic manner with increasing solid fractions. This was shown by constructing simple geometric 2D and 3D unit cells. Furthermore, the inter-particle necks were modeled by considering the overlap between the particles. It could be shown that with increasing overlaps, the pore sizes decreased. The overlapping sphere model was used to investigate the effect of considering the string of pearls and the overlap therein to model the local mechanical properties of the pore walls against the use of a constant cross section. It could be shown that assuming the string of pearls as a constant cross section would result in too sooner prediction of failure due to stretching and bending, while a delayed prediction of pore collapse due to buckling. It was also shown that the smaller the overlap, on the one hand, the higher the axial and bending stress, while on the other hand, the smaller the critical buckling load. Moreover, the critical buckling load was shown to scale linearly with the amount of overlap. Thus, accounting for the string of pearls in a pearl-necklace-like network is significantly more important than previously considered.

ACKNOWLEDGMENTS

S.A. acknowledges the DLR-DAAD Doctoral Research Fellowship.

AUTHOR DECLARATIONS

Conflict of Interest

The authors have no conflicts to disclose.

Author Contributions

Ameya Rege: Conceptualization (equal); Formal analysis (lead); Investigation (lead); Methodology (equal); Supervision (lead); Validation (lead); Visualization (lead); Writing – original draft (lead). **Shivangi Aney**: Methodology (supporting); Validation (supporting); Visualization (supporting). **Lorenz Ratke**: Conceptualization (equal); Formal analysis (supporting); Methodology (equal); Writing – review & editing (lead).

DATA AVAILABILITY

The data that support the findings of this study are available from the corresponding author upon reasonable request.

REFERENCES

[1] L. J. Gibson, M. F. Ashby, G. S. Schajer, and C. I. Robertson, "The mechanics of two-dimensional cellular materials," Proc. R. Soc. London, Ser. A **382**, 25–42 (1982).

[2] L. J. Gibson and M. F. Ashby, "The mechanics of three-dimensional cellular materials," Proc. R. Soc. London, Ser. A **382**, 43–59 (1982).

[3] S. F. Plappert, J.-M. Nedelec, H. Rennhofer, H. C. Lichtenegger, and F. W. Liebner, "Strain hardening and pore size harmonization by uniaxial densification: A facile approach toward superinsulating aerogels from nematic nanofibrillated 2,3-dicarboxyl cellulose," Chem. Mater. **29**, 6630–6641 (2017).

[4] A. Rege, S. Aney, and B. Milow, "Influence of pore-size distributions and pore-wall mechanics on the mechanical behavior of cellular solids like aerogels," Phys. Rev. E **103**, 043001 (2021).

[5] S. Aney and A. Rege, "The effect of pore sizes on the elastic behaviour of open-porous cellular materials," Math. Mech. Solids (published online, 2022).

[6]A. Rege, M. Schestakow, I. Karadagli, L. Ratke, and M. Itskov, "Micro-mechanical modelling of cellulose aerogels from molten salt hydrates," Soft Matter **12**, 7079–7088 (2016).
[7]A. Rege, I. Preibisch, M. Schestakow, K. Ganesan, P. Gurikov, B. Milow, I. Smirnova, and M. Itskov, "Correlating synthesis parameters to morphological entities: Predictive modeling of biopolymer aerogels," Materials **11**, 1670 (2018).
[8]M. Schwan, R. Tannert, and L. Ratke, "New soft and spongy resorcinol-formaldehyde aerogels," J. Supercrit. Fluids **107**, 201–208 (2016).
[9]J. Lei and Z. Liu, "A novel constitutive model for the mechanical properties of silica aerogels," J. Appl. Phys. **124**, 025102 (2018).
[10]S. Aney, J. Schettler, M. Schwan, B. Milow, and A. Rege, "Insights into the micromechanics of organic aerogels based on experimental and modeling results," Adv. Eng. Mater. **24**, 2100095 (2022).
[11]H.-S. Ma, A. P. Roberts, J.-H. Prévost, R. Jullien, and G. W. Scherer, "Mechanical structure-property relationship of aerogels," J. Non-Cryst. Solids **277**, 127–141 (2000).
[12]R. Abdusalamov, C. Scherdel, M. Itskov, B. Milow, G. Reichenauer, and A. Rege, "Modeling and simulation of the aggregation and the structural and mechanical properties of silica aerogels," J. Phys. Chem. B **125**, 1944–1950 (2021).
[13]A. Halperin and P. M. Goldbart, "Early stages of homopolymer collapse," Phys. Rev. E **61**, 565–573 (2000).
[14]S. Majumder, U. H. E. Hansmann, and W. Janke, "Pearl-necklace-like local ordering drives polypeptide collapse," Macromolecules **52**, 5491–5498 (2019).
[15]A. Emmerling, J. Gross, R. Gerlach, R. Goswin, G. Reichenauer, J. Fricke, and H.-G. Haubold, "Isothermal sintering of SiO_2-aerogels," J. Non-Cryst. Solids **125**, 230–243 (1990).
[16]J. Groß and J. Fricke, "Scaling of elastic properties in highly porous nanostructured aerogels," Nanostruct. Mater. **6**, 905–908 (1995).
[17]R. M. Christensen, "Mechanics of cellular and other low-density materials," Int. J. Solids Struct. **37**, 93–104 (2000).
[18]Z. Chen, X. Wang, F. Giuliani, and A. Atkinson, "Microstructural characteristics and elastic modulus of porous solids," Acta Mater. **89**, 268–277 (2015).
[19]R. Dargazany and M. Itskov, "Yield behavior of colloidal aggregates due to combined tensile-bending loads," Phys. Rev. E: Stat., Nonlinear, Soft Matter Phys. **85**, 051406 (2012).
[20]R. Dargazany, A. Rege, and M. Itskov, "Elasticity of colloidal clusters with application to carbon-black aggregates in filled rubbers," in *Constitutive Models for Rubber VIII* (CRC Press, 2013), pp. 261–266.
[21]R. Dargazany, H. Chen, J. Lin, A. I. Azad, and A. Alexander-Katz, "On the validity of representation of the inter-particle forces of a polymer-colloid cluster by linear springs," Polymer **109**, 266–277 (2017).
[22]S.-J. L. Kang, *Sintering Densification, Grain Growth and Microstructure* (Elsevier, Amsterdam, NL, 2005).
[23]G. W. Scherer, "Sintering aerogels," J. Sol-Gel Sci. Technol. **13**, 937–943 (1998).
[24]D. M. Smith, G. W. Scherer, and J. M. Anderson, "Shrinkage during drying of silica gel," J. Non-Cryst. Solids **188**, 191–206 (1995).
[25]S. Smitha, P. Shajesh, P. R. Aravind, S. R. Kumar, P. K. Pillai, and K. G. K. Warrier, "Effect of aging time and concentration of aging solution on the porosity characteristics of subcritically dried aerogels," Microporous Mesoporous Mater. **91**, 286–292 (2006).
[26]F. He, H. Zhao, X. Qu, C. Zhang, and W. Qiu, "Modified aging process for silica aerogel," J. Mater. Process. Technol. **209**, 1621–1626 (2009).
[27]L. Cipeletti, S. Manley, R. Ball, and D. Weitz, "Universal aging features in the restructuring of fractal colloidal gels," Phys. Rev. Lett. **84**, 2275–2278 (2000).
[28]G. Reichenauer, "Thermal aging of silica gels in water," J. Non-Cryst. Solids **350**, 189–195 (2004).
[29]G. W. Scherer, "Structure and properties of gels," Cem. Concr. Res. **29**, 1149–1157 (1999).
[30]R. Strom, Y. Masmoudi, A. Rigacci, G. Petermann, L. Gullberg, B. Chevalier, and M.-A. Einarsrud, "Strengthening and aging of wet silica gels for up-scaling of aerogel preparation," J. Sol-Gel Sci. Technol. **41**, 291–298 (2007).
[31]H. Omranpur and S. Motahari, "Effects of processing conditions on silica aerogel during aging: Role of solvent, time and temperature," J. Non-Crystallline Solids **379**, 7–11 (2013).
[32]L. J. Gibson and M. F. Ashby, *Cellular Solids: Structure and Properties*, Cambridge Solid State Science Series, 2nd ed. (Cambridge University Press, 1997).